The Astrophysical Journal, 855:40 (11pp), 2018 March 1 https://doi.org/10.3847/1538-4357/aaaf1b

Investigating the Effect of IMF Path Length on Pitch-angle Scattering of Strahl within 1 au

G. A. Graham[1], I. J. Rae[1], C. J. Owen[1], and A. P. Walsh[2]
[1] University College London, Department of Space and Climate Physics, Mullard Space Science Laboratory, Dorking, Surrey RH5 6NT, UK
[2] European Space Astronomy Centre, Urb. Villafranca del Castillo, E-28692 Villanueva de la Cañada, Madrid, Spain
Received 2017 September 15; revised 2018 January 8; accepted 2018 February 11; published 2018 March 6

Abstract

Strahl is the strongly field-aligned, beam-like population of electrons in the solar wind. Strahl width is observed to increase with distance from the Sun, and hence strahl electrons must be subject to in-transit scattering effects. Different energy relations have been both observed and modeled for both strahl width and the width increase with radial distance. Thus, there is much debate regarding what mechanism(s) scatter strahl. In this study, we use a novel method to investigate strahl evolution within 1 au by estimating the distance traveled by the strahl along the interplanetary magnetic field (IMF). We do this by implementing methods developed in previous studies, which make use of the onset of solar energetic particles at ∼1 au. Thus, we are able to obtain average strahl broadening in relation to electron energy and distance, while also taking into account the general effect of IMF topology and adiabatic focusing experienced by strahl. We find that average strahl width broadens with distance traveled along the IMF, which suggests that strahl width is related to the path length taken by the strahl from the Sun to 1 au. We also find that strahl pitch-angle width broadening per au along the IMF length increased with strahl energy, which suggests that the dominant strahl pitch-angle scattering mechanism likely has an inherent energy relation. Our pitch-angle broadening results provide a testable energy relation for the upcoming *Parker Solar Probe* and *Solar Orbiter* missions, which are both set to provide unprecedented new observations within 1 au.

Key words: plasmas – scattering – solar wind – Sun: heliosphere

1. Introduction

The solar wind is generally considered to have three constituent electron populations: a thermal "core," a suprathermal "halo," and a suprathermal "strahl" (e.g., Feldman et al. 1975; Maksimovic et al. 2005). Studies, such as those referenced above, also find that core and halo populations are typically relatively isotropic compared to strahl, which is a strongly field-aligned beam of electrons. Strahl electrons travel in the anti-sunward direction, along the interplanetary magnetic field (IMF), at high velocities relative to the bulk plasma flow and are most often observed in either the parallel or anti-parallel magnetic field direction, depending on the IMF polarity (e.g., Feldman et al. 1978; Pilipp et al. 1987a). However, certain IMF topologies, such as a closed loop with both IMF footpoints connected to the solar surface, can result in bi-directional strahl, in which electron beams are observed in both the parallel and anti-parallel magnetic field direction simultaneously (e.g., Gosling et al. 1987). It is also possible to observe local sunward strahl due to folded IMF topologies (e.g., Owens et al. 2013, and references within). Finally, it should be noted that there are also times when no clear strahl population is observed in the solar wind (e.g., Anderson et al. 2012), particularly during observations in the slow solar wind (e.g., Gurgiolo & Goldstein 2017).

Strahl beams observed at 1 au have pitch-angle widths that are often significantly larger than predicted than to be due purely to expansion effects and is frequently >20° (e.g., Owens et al. 2008; Anderson et al. 2012; Graham et al. 2017). Hence, adiabatic focusing cannot be the sole effect experienced by the suprathermal electrons in the solar wind. The presence of this broader strahl and a near-isotropic halo population at 1 au is thus frequently explained as a result of scattering of suprathermal electrons via wave–particle interactions in transit or by global reflection in the heliosphere (e.g., Pagel et al. 2007; Saito & Gary 2007; Landi et al. 2012; Smith et al. 2012; Pavan et al. 2013). In general, strahl pitch-angle width has also been observed to increase with heliospheric radial distance beyond 1 au (Hammond et al. 1996; Graham et al. 2017). The fractional density of strahl electrons relative to total electron density has also been observed to decrease with heliospheric radial distance, while that of the halo electrons increases (e.g., Maksimovic et al. 2005; Stverak et al. 2009). This implies that strahl electrons are indeed subject to some form of in-transit scattering process, or processes, as they travel outward away from the Sun and that, eventually, they are fully scattered to form part of the quasi-isotropic halo population.

At this point, we should note that some studies have also demonstrated that there are conditions under which electron behavior could differ from the in-transit concept discussed above. For example, it has been shown that the halo population could form in the low corona near sector boundaries, before subsequent adiabatic focusing results in the formation of a strahl beam, the diffuse nature of which could then be preserved though scattering effects (Che & Goldstein 2014). It has also been shown that a broad strahl-like feature could be produced by pitch-angle scattering in the solar wind of a halo population with a large drift relative to the core (Seough et al. 2015). It is also important to consider kinetic modeling investigations of strahl evolution, such as Lie-Svendsen et al. (1997) and Horaites et al. (2017). The former compared their results to *Helios* observations at 0.3 au, and the latter compared their results to *Wind* observations at 1 au. These two studies

both demonstrated that the kinetic approach can explain the formation of a strahl beam in fast solar wind streams. In particular, narrow strahl with beam widths of ∼10°–50° can be modeled effectively and that the resulting strahl energy relation is a decrease in width with electron energy.

Thus, the origins of both the suprathermal field-aligned strahl and the approximately isotropic halo remain unclear. It should be noted that each of the models cited above used specific conditions in their study. For example, Smith et al. (2012) used coronal hole wind with a strong magnetic field gradient, whereas Che & Goldstein (2014) used approximations appropriate for very slow wind observed near sector boundaries. In order to better understand the coronal origins of strahl and halo electrons, we must thus determine what processes affect the solar wind electrons in transit.

Previous studies at ∼1 au have examined the relationship between strahl width and electron energy to understand the nature of the strahl scattering mechanism(s), in particular the role of resonant wave–particle interactions. However, these studies have rendered a number of different, seemingly contradictory, findings, which suggest that there may be multiple scattering mechanisms at play. Strahl beams have been observed to have pitch-angle widths that decrease with increasing electron energy (e.g., Feldman et al. 1978; Pilipp et al. 1987a; Fitzenreiter et al. 1998). The opposite relation has also been reported during solar wind intervals with enhanced magnetic field fluctuations (Pagel et al. 2007). In addition, a statistical study completed using 4 yr of solar wind data found that, at any given time, it is equally probable for strahl width to increase or decrease with increasing electron energy (Anderson et al. 2012).

Some studies have also observed that strahl pitch-angle distributions are generally narrower in the fast solar wind than the slow solar wind (Feldman et al. 1978; Pilipp et al. 1987b; Fitzenreiter et al. 1998). However, it has also been shown that proximity to IMF sector boundaries may have a more significant effect on strahl width than wind speed, producing a strahl pitch-angle broadening effect that is independent of electron energy (Pilipp et al. 1987b). Finally, it is also unclear whether the strahl scattering processes operate continuously or intermittently throughout the heliosphere (e.g., Gurgiolo et al. 2012). There are a wide range of proposed candidates for strahl scattering mechanisms that result in a number of different strahl width energy relations. Examples include, but are not limited to, whistler-mode waves resulting from temperature anisotropy, turbulent cascade, or heat flux instability; strahl-generated Lagmuir waves; and/or obliquely propagating kinetic Alfvén waves. We examine these potential scattering mechanisms in more detail in the discussion.

Studying the evolution of strahl electrons with heliospheric radial distance can help to separate the effects of in-transit solar wind processing from the original coronal electron distributions. Previous investigations have studied the evolution of strahl width beyond 1 au, demonstrating that strahl beam width broadens with heliospheric radial distance (Hammond et al. 1996; Graham et al. 2017), and studies of suprathermal electrons within 1 au indicate that strahl is scattered to form halo electrons (e.g., Maksimovic et al. 2005; Stverak et al. 2009). *Helios* observations of strahl width at different radial distances have been made within 1 au, but the general relation between strahl width and distance was not determined (Pilipp et al. 1987b). However, a strong correlation between strahl width and the sector structure of the IMF was found, with strahl electrons displaying increased width near boundaries for all electron energies (Pilipp et al. 1987b).

Narrow strahl features (<20°) are most commonly observed in the coronal hole solar wind (e.g., Fitzenreiter et al. 1998; Anderson et al. 2012). This suggests either that the strahl has undergone a lesser degree of scattering in transit within the fast solar wind than the slow or that the different origins of the slow and fast solar wind result in different electron velocity distributions. It has also been shown that narrow strahl features are fractionally more likely to occur for counter-streaming strahl within interplanetary coronal mass ejections (ICMEs) than in the solar wind as a whole (e.g., Anderson et al. 2012). ICMEs and the fast solar wind do not generally originate from similar source regions. However, both ICMEs, which frequently experience overexpansion as they propagate (Gosling et al. 1994), and high-speed coronal hole wind should have a greater decrease in IMF strength per unit distance along the IMF direction than the slow solar wind (e.g., Gosling et al. 1994; Anderson et al. 2012). This provides a greater adiabatic focusing effect for the strahl scattering mechanism to overcome. Therefore, it seems likely that the topology of the IMF and specifically the path length traveled by the strahl electron should have a significant effect on the width of the strahl observed at 1 au. If an average IMF length along which the strahl has traveled can be reliably estimated, then information pertaining to the strahl scattering mechanisms in relation to electron energy and distance can be obtained, which then takes into account the effect of the IMF topology and adiabatic focusing experienced by the electrons. In this study we will estimate the path length traveled by the strahl electrons along the IMF and examine its relation to the average observed width of the strahl.

2. Method

Figure 1 shows an illustration of the methods used in this study. We use electron and ion solar energetic particle (SEP) onset time observations at ∼1 au associated with solar flares and type III radio bursts to calculate the IMF path lengths traveled by the field-aligned SEPs. We thus estimate the path length traveled by the field-aligned strahl from the Sun to 1 au. We then find the average strahl beam width observed immediately before the onset times for each strahl energy and examine the width of the strahl as a function of the IMF path length. Finally, we investigate the properties of the solar wind and magnetic field for each event, in order to understand possible global or local effects on the strahl beam.

2.1. Data

In this study we use an independently derived list of 69 SEP events and associated phenomena originally studied by Nitta et al. (2006), which were determined to be impulsive events with associated observed type III radio bursts. In addition, Nitta et al. (2006) also investigated the source regions of the SEP events and found that ∼80% of the events were in close proximity to source regions with open magnetic flux. In this study we use observations from the *Wind* spacecraft three-dimensional plasma (3DP) instrument.

We investigate solar wind electrons using the *WIND* 3DP Electron Electrostatic Analyzers (EESAs), which have an energy range of 3 eV–30 keV and complete 32 energy sweeps

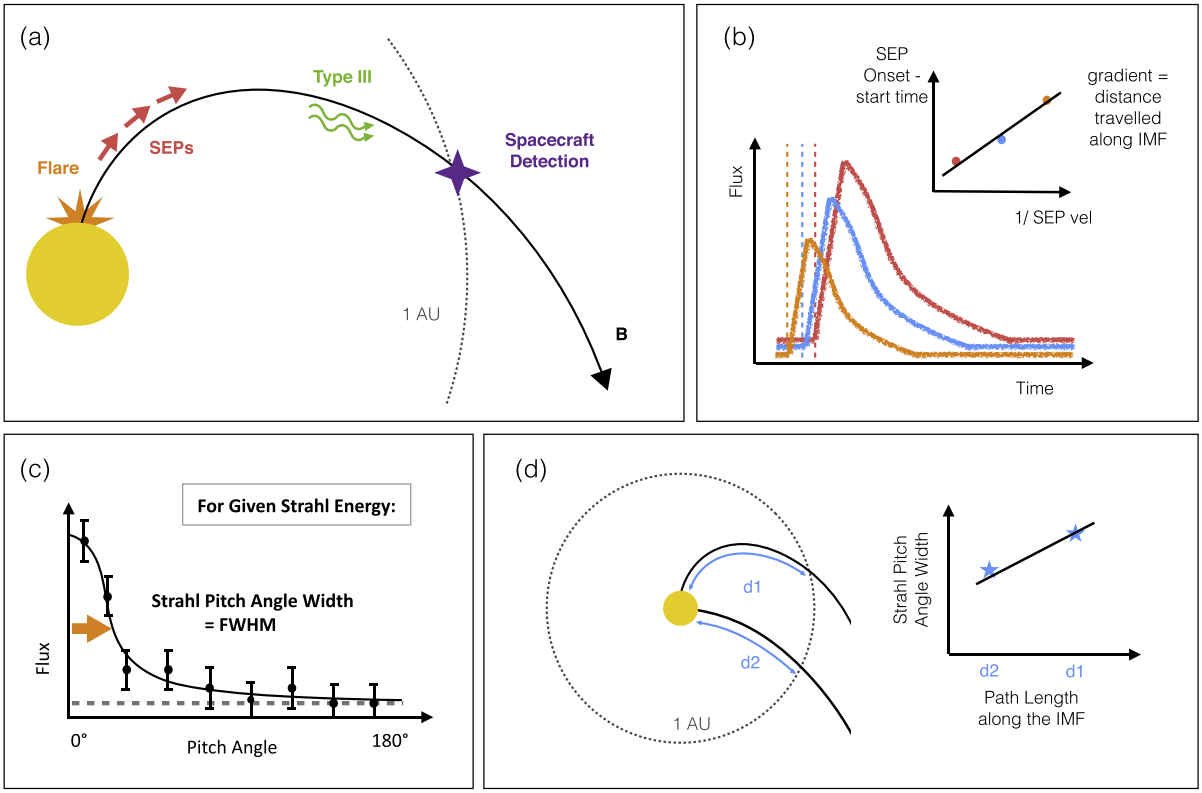

Figure 1. Key aspects of the methods used in this study to determine SEP onset times, estimate IMF length, and compare with average strahl width. (a) Illustration of an impulsive SEP event and associated phenomena. SEPs are accelerated on an open Earth-directed IMF line, travel along the IMF, and are detected by the spacecraft at 1 au. (b) Illustration of the observed increase in energetic particle flux at 1 au for three different energies: low (red), medium (blue), and high (orange). The dashed lines show the SEP onset times. The top corner inset shows an illustration of these onset times as a function of inverse SEP velocity. This inset shows the expected velocity dispersion, with faster particles arriving first. (c) Illustration of fitting to average electron pitch-angle distribution for one suprathermal energy bin. Strahl beam width is given by the FWHM of the Gaussian peak at either 0° pitch angle or 180° depending on the IMF orientation. The gray dashed line represents a constant background. (d) Illustration of the expected trend if there is a clear relationship between strahl beam width and distance traveling along the IMF path length, i.e., if the scattering rate is constant with time and distance traveled along the field away from the Sun. The shorter distance d2 means that strahl would take a shorter time to travel the same radial distance as d1. Hence, field-aligned strahl electrons would experience the same adiabatic focusing but greater scattering effects.

per ~3 s spacecraft spin (Lin et al. 1995). Higher-energy SEP electrons were investigated using the *Wind* 3DP Solid State Telescopes (SSTs), which have an energy range of 25 keV–1 MeV and 16 times per spacecraft spin (Lin et al. 1995). However, the time resolution of the available data for both the EESA and SSTs varies depending on the instrument mode available at the time of observation. Helium ions were investigated using the *Wind* 3DP Energetic Particles: Acceleration, Composition, and Transport (EPACT) instrument, specifically the Low Energy Matrix Telescopes (LEMTs), which have an energy range of 1.4–10 MeV/nuc and data that are generally available at a time resolution of 5 minutes (Von Rosenvinge et al. 1995). Finally, magnetic field fluctuations are examined using the *Wind* 3 s magnetometer (MAG) data (Lepping et al. 1995). Any additional information, such as solar wind speed, was obtained using NASA OMNI data (King & Papitashvili 2005). The Nitta et al. (2006) events were visually inspected to verify the location of the *Wind* spacecraft. A number of the Nitta et al. (2006) events were then discarded from our analysis, as examination of spacecraft position and plasma parameters suggested either that the *Wind* spacecraft was situated in the magnetosphere or that there was ambiguity regarding the purity of the solar wind observed, for example, due to proximity to the foreshock.

2.2. Why Estimate IMF Length Using SEP Onsets?

On average the IMF structure agrees with the Parker solar wind model, but observations have also shown that the ecliptic magnetic field angle can significantly deviate from the expected spiral field direction (e.g., Forsyth et al. 1996; Owens et al. 2008, 2013; Borovsky 2010). This means that a Parker model IMF on its own is not sufficient for the accurate estimation of field line length required in this study. As an aside, this may also partly explain why, although strahl width is generally broader in the slow wind, there is no direct correlation between solar wind speed and strahl width (Pilipp et al. 1987b). However, it is possible to use the onset time of SEP events to estimate the IMF length traveled by energetic particles along the field (e.g., Krucker et al. 1999). Hence, in this paper we use methodology developed in SEP studies to estimate the path length traveled by the field-aligned SEPs and therefore estimate the path length traveled along the same field lines by strahl from the Sun to 1 au.

In this study we select and analyze impulsive SEP events, as, in general, they are spatially and temporally less extensive than gradual events. For example, Reames (1999) estimated a "source longitude" spread of ±20° for flux tubes containing promptly arriving impulsive SEPs, compared to that of the entire face of the Sun for gradual events. In particular, ions

accelerated at solar flares are observed to be well confined to flux tubes connected to the reconnection site (Mazur et al. 2000). It has also been observed that impulsive SEPs are associated with solar flares and with reconnection with open magnetic field lines that are magnetically well connected to the observer (Reames 2013, and references within). Some of these studies also found that impulsive SEPs are also associated with type III radio bursts related to the transport of accelerated 10–1000 keV electrons. Type III radio bursts can be a useful proxy for the "start time" of the SEP event (Tan et al. 2013). It is important to note that impulsive SEPs from the same source have been observed to have a spread of >130° (Wiedenbeck et al. 2011), implying that SEPs may experience significant perpendicular transport. However, a recent investigation into an impulsive SEP event, in which the two *STEREO* spacecraft observed SEPs on opposite polarity field lines, found that the most likely explanation was particle propagation along nonradial magnetic field toward both spacecraft magnetic solar footpoints (Klassen 2017). Hence, widely spread impulsive SEPs may be a result of complex reconnection topology on the Sun as opposed to scattering effects. Hence, with careful examination of the events, we can use SEPs to estimate IMF path length.

2.3. Determining SEP Onsets

We examined high-energy electron and helium SEP fluxes for the days associated with each cataloged type III radio burst from Nitta et al. (2006). We chose to use two different particle species, electrons and helium ions, as electrons behave differently from ions as they resonate with different wave modes. Hence, by comparing path lengths estimated using both, we are able to verify whether wave–particle interactions affect our IMF length estimates. In order to find the onset times for the SEP events, we used the same method as outlined in the Krucker et al. (1999) study. For each species and for each energy, we normalize the particle flux relative to the background flux in units of standard deviation. This enabled clear observation of any increase in energetic particle flux associated with the type III radio burst. We then determine an upper, or latest, limit for the onset time by locating the time at which the particle flux increases to 6σ above the background level; at any time beyond this limit the SEP event has definitely started (Krucker et al. 1999). The onset time is taken to be the first preceding time, relative to the upper limit, at which the normalized flux rises above the background level (Krucker et al. 1999). The difference between the upper limit and the onset time was used as an estimate of the onset uncertainty. Examples of SEP onset times obtained for this study are shown in Figure 2. In the original Krucker et al. (1999) study, all onset times and uncertainties were also determined by eye for each individual event, and it was found that the results were consistent with the automated method.

2.4. Estimating IMF Path Length

Once the onsets for each species and for each energy were determined, we performed velocity dispersion analysis (VDA) to estimate the IMF path length traveled by the particles, as shown schematically in panel (b) of Figure 1. VDA makes use of the different time of flight of different velocity SEPs, with the assumption that they are released at the same time and location. The gradient of onset time as a function of the inverse

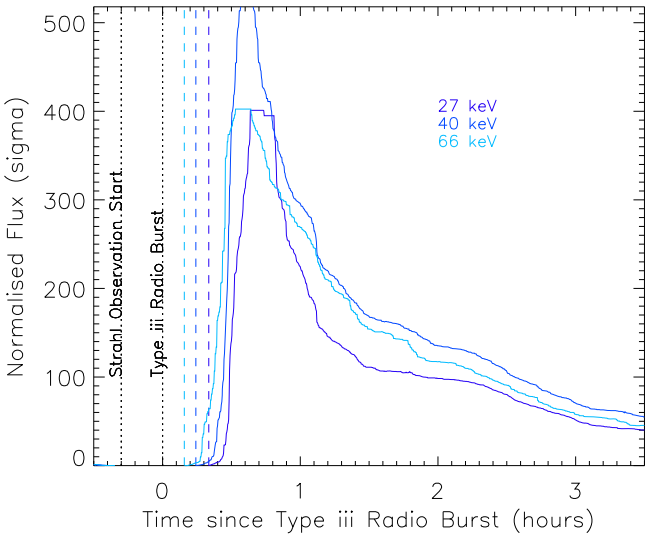

Figure 2. Example of SEP onset time detection for electron SEPs with energies of ~27, 40, and 66 keV. The plot shows normalized SEP electron flux as a function of time since the associated type III radio burst onset. The SEP electron flux is normalized in units of standard deviation relative to the background flux for each energy. Onset times for each energy are marked by the vertical dashed lines in the corresponding color. The type III radio burst onset time is marked by a dotted and labeled line. The average strahl pitch-angle width (see Section 2.5) is found for the 20 minutes before the observed type III radio burst onset.

of the particle velocity can then be used as an estimate of the length along the IMF traveled by the SEPs (e.g., Tan et al. 2013). This method also assumes that the first SEPs to arrive travel scatter-free (i.e., mean free path >1 au) to the observation point, resulting in enhancements in particle flux that display velocity dispersion.

Ion VDA has generally been found to give reasonable estimates of IMF path length, but VDA for electron SEPs may result in unphysically short path lengths (i.e., less than 1 au) (Tan et al. 2013). Previous studies have suggested that these short path lengths may be an effect of energy deposition in the solid-state telescopes on the *Wind* spacecraft, which would result in an apparent increase in flux for the lower-energy bins earlier than expected and shorten the path length estimate (Tan et al. 2013). However, energy deposition should not be an issue if the intensities are high enough (Haggerty & Roelof 2002). Hence, before conducting analysis using the electron SEP onset times, we first compared the SST observations to those of the EESA observations for the overlapping electron SEP energy bin. We found that for events where both instruments detected clear onsets, the path lengths agreed well, and therefore short path lengths were not likely to be an instrumental effect.

Another possible explanation for an unphysically short path length estimate may be that higher-energy SEP electrons are subject to scattering effects and therefore arriving later than expected. Previous studies have shown that this effect may be due to the transition from a scatter-free to diffusive regime as the electron SEP energy approaches relativistic values (e.g., Tan et al. 2011). It has been shown that higher-energy SEP electrons, approaching the diffusive regime, are scattered more than lower-energy electrons and that the boundary between the two regimes varies from event to event (e.g., Tan et al. 2013). Hence, we do not use VDA when we estimate the IMF path length using electron SEPs. Instead, we estimated the IMF path length using the time taken for electron SEPs of ~27 keV to

travel from the Sun to ~1 au. It is possible to estimate the "start time" of the SEP event, as type III radio bursts are related to the transport of accelerated 10–1000 keV (Tan et al. 2013). Thus, we can assume that the time taken for the field-aligned electron SEP to travel along the IMF path length is the time difference between the onset of the type III radio burst and the onset of the ~27 keV electron SEPs.

The VDA method for helium ion SEPs and the travel time method for electron SEPs and type III bursts (outlined above) were both used to calculate IMF path length estimates for each event. Any IMF path length estimates that resulted in large errors (found from fitting in the VDA case, and propagated through in the travel time case) were visually inspected, and any errors that exceeded 1 au or 0.3 times the calculated IMF path length were excluded from further analysis. We also excluded any estimates with a nonphysical, negative IMF length. Using these criteria, we exclude results pertaining to unclear onset determination or to unclear velocity dispersion. Key reasons for these unclear VDA distributions include high-energy SEPs arriving later than expected relative to lower-energy SEPs, potential overlapping SEP events, or unclear or absence of onset detection for some or all energies.

We then compared the estimated IMF path lengths for both the ions and the electrons with the average strahl width. Figure 1(d) illustrates the expected trend if there is a clear relationship between strahl beam width and distance traveled along the IMF. This could occur if the scattering rate is constant with time and distance from the Sun. The shorter distance along the field, d2, means that strahl would take a shorter time to travel the same radial distance as the longer distance along the field, d1. Hence, the strahl electrons would experience the same adiabatic focusing but may undergo a greater scattering effect.

2.5. Determining Strahl Beam Width

The average electron pitch-angle distribution, for each suprathermal energy bin, was determined for 20 minutes before each radio burst detection. Strahl beam widths were determined by fitting a function consisting of the sum of two Gaussians, one centered on 0° pitch angle and the other on 180°, and a constant background (for more information regarding method see, e.g., Graham et al. 2017). Gausian fitting has been used previously in observational investigations (e.g., Hammond et al. 1996; Anderson et al. 2012), and strahl pitch-angle distributions have been shown to be approximately Gaussian (Horaites et al. 2017). The FWHM of the fitted peaks was then used as a measure of beam width, while the constant term accounts for a background halo population. The assumption that the halo is an approximately isotropic population means that the fitting method employed in this study does not consider potential halo anisotropies. However, we only examine strahl fitting results where the peak is at least 2 times greater than that of the background to minimize the effects of ambiguous pitch-angle distributions (e.g., Anderson et al. 2012; Graham et al. 2017). We also require that the FWHM of the peak must be $<180°$ in order to be considered a strahl beam, as larger widths represent an almost isotropic distribution (e.g., Hammond et al. 1996; Anderson et al. 2012). An illustration of the strahl fitting technique is shown in panel (c) of Figure 1.

2.6. Magnetic Field Fluctuations

We also examine the magnetic variation both during the strahl observations and during the entire period in which SEP onsets are observed, in order to investigate possible effects related to magnetic fluctuations. To do this, we used a quantity referred to as partial variance of increments (PVI; Osman et al. 2014):

$$\mathrm{PVI} = \frac{|\Delta \boldsymbol{B}|}{\sqrt{\langle |\Delta \boldsymbol{B}|^2 \rangle}}, \quad (1)$$

where $\Delta \boldsymbol{B}$ is the change in magnetic field between 3 s measurements and the average is taken over 30 minutes, which corresponds roughly to the timescale where solar wind turbulent fluctuations become uncorrelated (Osman et al. 2014). We note that 3 s observations cannot provide information on intermittent features at kinetic scales. However, they may provide useful information with regard to possible blurring of the strahl distribution due to magnetic field fluctuations during strahl observation periods, or strahl scattering resulting from coherent non-Gaussian magnetic field structures such as current sheets between solar wind flux tubes.

3. Results

The strahl width as a function of energy observed at a given time for each interval studied produced a variety of results. We observed events where the average strahl width broadened with energy, events where it decreased with energy, and events with unclear or no energy relation. This is in line with the variable nature of strahl reported by previous studies, particularly Anderson et al. (2012), which found that at a given time the strahl width may broaden or narrow with energy. However, in this investigation we focus our discussion on the relationship between average strahl width and IMF length, as well as the energy relation for beam broadening with heliospheric distance.

The IMF path length was estimated using the travel time method for ~27 keV electron SEPs and type III bursts (outlined in Section 2.4) and compared to the average strahl width (outlined in Section 2.5). The results are shown in the left panels of Figure 3, which show the average strahl pitch-angle width as a function of estimated IMF path length for suprathermal energy bins ranging from ~140 to 1300 eV. We observed an increase in average strahl width with estimated IMF length for all strahl energies, with higher-energy strahl displaying a more pronounced relationship, except perhaps in the highest strahl energy channel, in which there is potentially a separation into two strahl populations—one with broader pitch-angle widths, and another with significantly narrower beam widths.

The IMF path length was also estimated using the VDA method for helium ion SEPs (outlined in Section 2.4) and compared to the average strahl width. The results are shown in the right panels of Figure 3, which show the average strahl pitch-angle width as a function of estimated IMF path length for suprathermal energy bins ranging from ~140 to 1300 eV. We again find an increase in average strahl width with IMF length, although the relationship is less clear. It should be noted that for the lowest strahl energy channel, for both IMF length estimation methods, we observe a weaker trend than for the higher energies, and further observations are required to resolve this ambiguity. There is also an event with a high estimate of

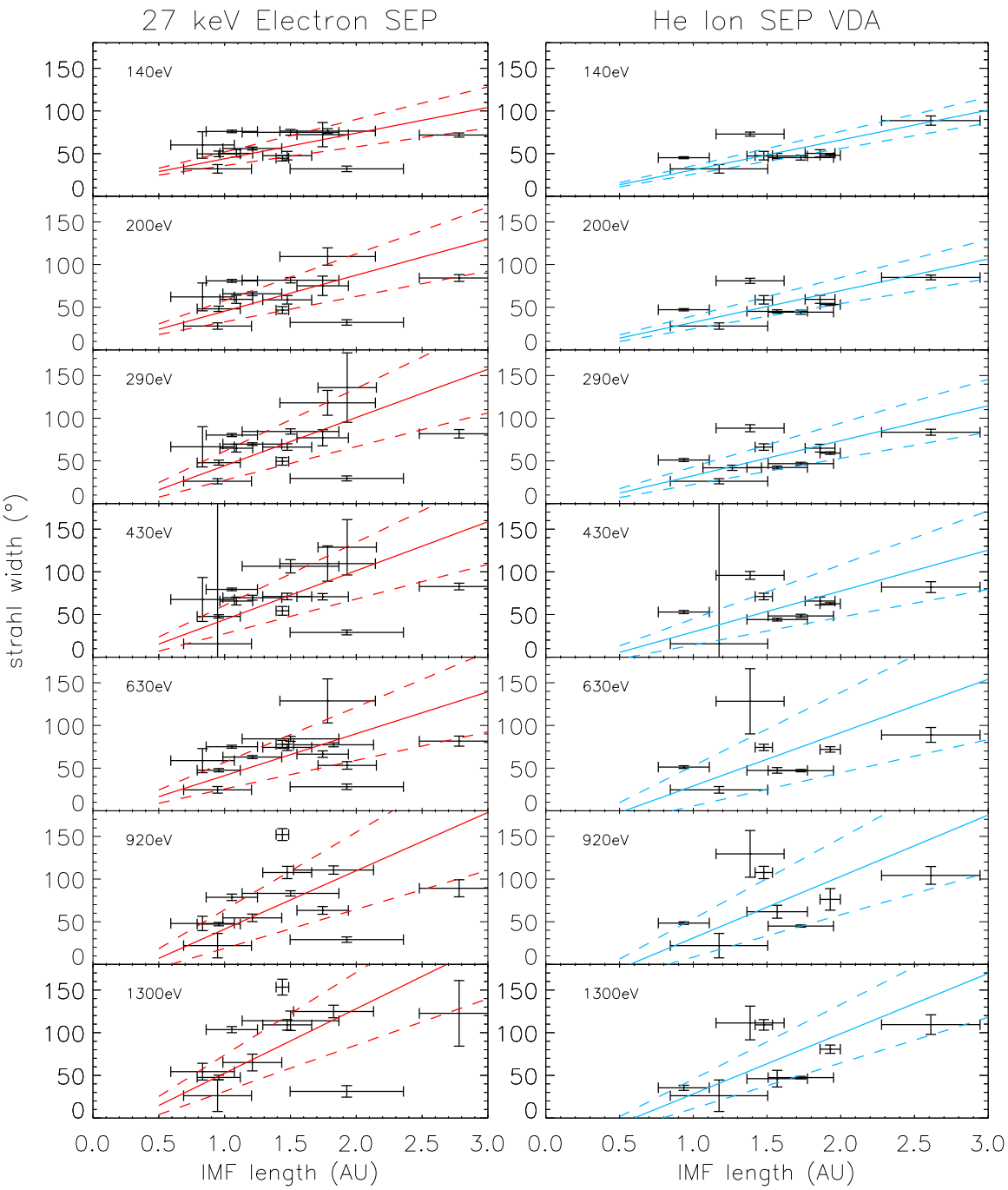

Figure 3. Average strahl pitch-angle width as a function of estimated IMF path length. Left: IMF path length found using the estimation method that assumes that the time between the onset of type III radio burst (proxy for SEP start times) and onset of the 27 keV electron SEPs is the time taken for the field-aligned 27 keV electron SEPs to travel along the IMF path length. Right: IMF path length estimated using He ion VDA. Each panel, for both the left and right columns, represents a different strahl electron energy, from top to bottom: ∼140, 200, 290, 430, 630, 920, and 1300 eV. The solid lines are linear fits to the data obtained using reduced major-axis regression, and the dashed lines are the calculated uncertainties for the linear fits (Isobe et al. 1990).

IMF length but narrow strahl that is observed in all energy channels in the left panels. This event is for a solar wind speed of ∼500 km s^{-1} and a relatively low median PVI of ∼0.46, but no evidence of any unusual solar wind conditions or ejecta were present.

We note that it was not possible to reliably estimate strahl width and IMF length for all of the initial 69 events. Nor do all events have an IMF estimate from both of the methods used in this study. After applying our fitting criteria for strahl observations and after removing IMF length estimates that had large errors or nonphysical results, we were only able to determine an estimate of both IMF length and strahl width for a subset of the initial list of events. The results in Figure 3 consist of 18 valid IMF estimates for the IMF lengths calculated using the travel time method and 13 valid IMF estimates for the VDA method. We can obtain IMF estimates from both methods for four events; two of these events render very similar IMF path lengths, and two do not. Given that there are only four events with results for both methods, we do not make any more quantitative assessment.

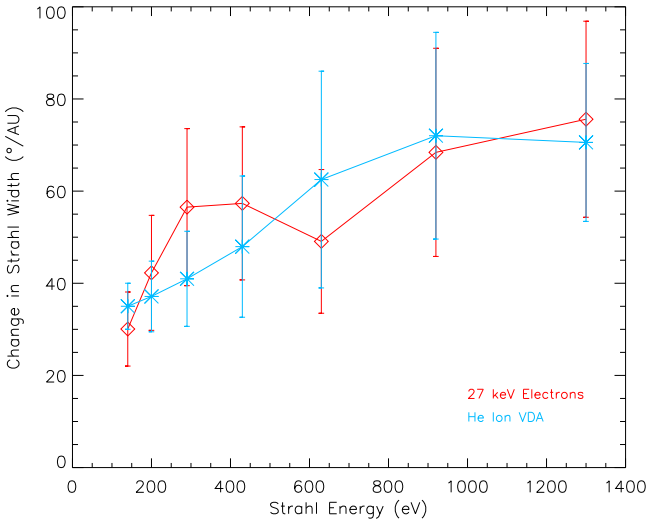

Figure 4. Change in strahl pitch-angle width per unit distance as a function of electron energy, obtained from linear fits to strahl width as a function of IMF path length in Figure 3. The relationship shown in red (diamonds) is found using the IMF path length estimation method that assumes that the time between the onset of type III radio burst (proxy for SEP start times) and onset of the 27 keV electron SEPs is the time taken for the field-aligned 27 keV electron SEPs to travel along the IMF path length. The relationship shown in blue (asterisks) is found using the IMF path length estimation method that uses He ion VDA. The error bars show the calculated uncertainties for the linear fits.

Analysis of the data using both IMF path length estimation methods shows an increase in average strahl width with IMF length, suggesting that for longer path lengths the strahl electrons are subjected to greater scattering effects. The two methods also produce some high values for IMF length, i.e., >2 au. However, even if these values are excluded, an increase in strahl width with estimated IMF length would be observed using both methods. At this point we should also consider that there could potentially be spatial effects leading to errors in our results for IMF path length. Mazur et al. (2000) found that He ions in impulsive events were well confined to "flux tubes." These flux tubes had an average estimated cross section of ∼0.03 au and a maximum cross section of ∼0.15 au. It is possible that as these flux tubes are convected outward from the Sun, they become tangled in transit with flux tubes with footpoints that are not connected to what will be the SEP acceleration site. Thus, as flux tubes convect across the spacecraft during an SEP event, we may also observe "empty" flux tubes that could affect our VDA. For each of our events, we calculated a length scale by dividing the time between the first and last observed SEP onsets by the average solar wind speed. The maximum value of this length scale was ∼0.08 au. Hence, we cannot completely rule out spatial effects, although no relationship between calculated length scale and large estimates of IMF path length was found.

The increase in average strahl pitch-angle width per unit distance along the IMF was obtained from linear fits to strahl width as a function of IMF path length, shown in Figure 3. This is shown as a function of suprathermal electron energy in Figure 4. The relationship shown in red (diamonds) is found using the IMF path length estimation method that assumes that the time between the onset of type III radio burst (proxy for SEP start times) and onset of the 27 keV electron SEPs is the time taken for the field-aligned 27 keV electron SEPs to travel along the IMF path length. The relationship shown in blue (asterisks) is found using the IMF path length estimation method that uses helium ion VDA. In both cases, we observe that strahl width broadening per unit distance along the IMF path is greater for higher strahl energies. The general trends for increase in strahl width per au for both methods are within error of each other, with a range of ∼30°–80°/au. We note at this point that the errors associated with our estimates of change in strahl width per unit distance are large. The increase in beam broadening per unit distance is also much clearer for lower-energy electrons; beyond ∼400 eV it is possible to interpret the trend as flat rather than increasing. However, even if the distribution is flat, the increase in strahl width is still larger than can be explained by a constant scattering rate in a simple time-of-flight model (Owens et al. 2008) or by kinetic modeling of strahl evolution to 1 au (Horaites et al. 2017).

The IMF topology, solar wind type, and IMF variation may all play a role in solar wind strahl width, and so each of these was examined. Figure 5 shows histograms of each of these parameters for all events investigated in this study. Panel (a) shows the model Parker spiral length calculated using observed average solar wind speed. The solid line represents the spiral length for a solar wind speed of 400 km s^{-1}, which is the average solar wind speed in the ecliptic (e.g., Hundhausen et al. 1970). In general, there is a difference of ∼29% between IMF lengths calculated using the Parker model and the IMF estimates calculated using the travel time method for electron SEPs. There is also generally a difference of ∼36% between IMF lengths calculated using the Parker model and the IMF estimates calculated using the VDA method. A comparison of IMF length estimates and theoretical Parker spiral lengths for each event is shown in Figure 6. Here we see that the results of the two aforementioned methods are reasonably similar given the low statistics. The IMF estimates calculated using the travel time method for electron SEPs are often lower than the theoretical Parker spiral lengths. However, in general, for both methods, the IMF length estimated is larger than the Parker length, usually by a significant amount.

We also compared the Parker angle calculated using average solar wind speed with average observed IMF angle, in the same manner as in the Forsyth et al. (1996) study using *Ulysses*. We found a peak around the expected Parker angle, but also some significant deviations where the observed field is nearly radial or tangential. Many such intervals have been previously observed in the solar wind (e.g., Forsyth et al. 1996; Borovsky 2010; Owens et al. 2013). For the probability distribution functions for IMF angle from 1965 to 2012 we refer the reader to Owens et al. (2013), where it is shown that generally the ideal Parker spiral values agree well with observations but that IMF direction is highly variable.

Panel (b) of Figure 5 shows the average observed solar wind speed during each of the events in this study. The average solar wind speed during these events varies from ∼300 to 600 km s^{-1}. The mean, median, and standard deviation for an event wind speed in this study are 416, 402, and 82 km s^{-1}, respectively. The solid line represents the spiral length for a solar wind speed of 400 km s^{-1}, which is the average solar wind speed in the ecliptic (e.g., Hundhausen et al. 1970). No direct relationship between strahl beam width and solar wind speed was observed. We also examined average solar wind speed for events with clearly detectable strahl versus those that did not fulfill the criteria specified in Section 2.5. It was found that events with measurable strahl beams had a higher mean value (e.g., 387 km s^{-1} for ∼140 eV strahl) than for those that

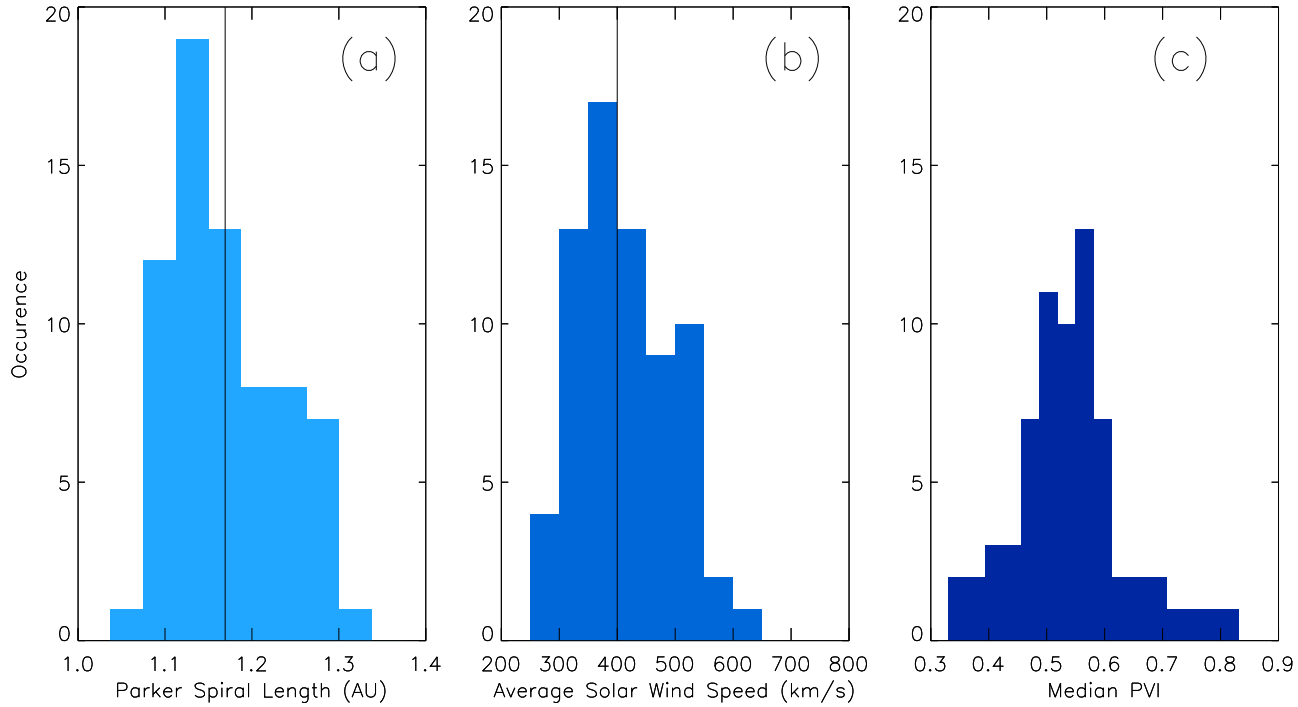

Figure 5. (a) Histogram for all events investigated in this study showing Parker spiral length calculated using observed average solar wind velocity. The solid line represents the spiral length for a solar wind speed of 400 km s^{-1}, which is the average solar wind speed in the ecliptic (Hundhausen et al. 1970). (b) Histogram for all events investigated in this study showing the average solar wind speed observed. (c) Histogram for all events investigated in this study showing the median PVI found for strahl observation time for each of the events investigated in this study. PVI values below 1 are considered to have minimal fluctuations (Osman et al. 2014).

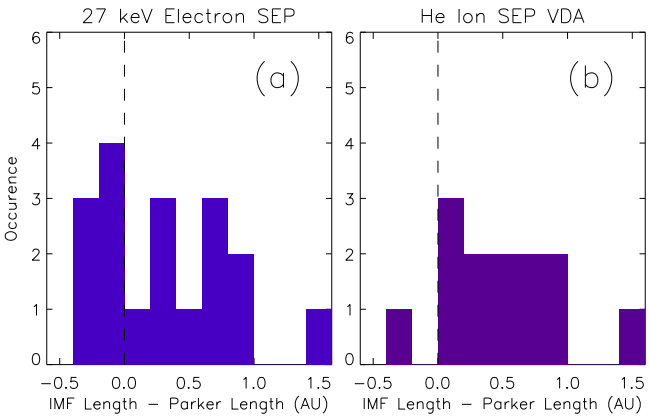

Figure 6. (a) Histogram for all events investigated in this study showing difference between the estimates of IMF path length using the travel time method for electron SEPs and type III bursts and the Parker spiral length calculated using observed average solar wind velocity. (b) Histogram for all events investigated in this study showing difference between the estimates of IMF path length using the VDA method for helium ion SEPs and the Parker spiral length calculated using observed average solar wind velocity.

had no measurable strahl beam (e.g., 431 km s^{-1} for ∼140 eV strahl), although they are both clearly slow solar wind. Panel (c) of Figure 5 shows the median PVI values calculated for each strahl observation period. The median values for PVI were found to be low (i.e., below 1.0) for the strahl observation periods (Osman et al. 2014). We examined the average strahl width for each event with both median and maximum values of PVI observed during each event. No relationship was observed in either case. We found no clear relationships between the solar wind parameters discussed above and strahl width (not shown). However, we do show the histograms of the general properties of the events in our study in order to provide context for the conditions under which our events were observed (see Figures 5 and 6).

4. Discussion

Estimates of IMF path length from the Sun to ∼1 au were calculated for each of the events examined in this study, using both the VDA method for helium ion SEPs and the travel time method for electron SEPs and type III bursts. Both methods give reasonable estimates of the IMF path length, which is in line with the previous results of Tan et al. (2013) and Mazur et al. (2000). For both IMF path length estimation methods used in this study, an increase in average strahl width with IMF length was observed. This relationship between strahl width and IMF path length suggests that strahl on longer IMF path lengths is subject to greater scattering effects en route from the Sun. We also observed that strahl broadening per au along the IMF path length significantly increases with increasing strahl energy, which suggests that pitch-angle scattering is greater for higher-energy strahl electrons. We note again here that it was not possible to reliably estimate strahl width and IMF length for all of the initial 69 events. In this investigation we tested and implemented a novel strahl width analysis technique and thus used an independently studied list of events as a staring point. A larger number of events would provide improved statistics and allow us to make more substantial claims regarding strahl broadening. However, our results do provide a good indication of the processes affecting the strahl within 1 au and a testable strahl width energy relation for both future inner heliospheric missions and further investigations.

Previous observational investigations into the evolution of strahl pitch-angle distributions found that, in general, strahl width increases with heliospheric radial distance and that strahl must be subjected to in-transit scattering effects (Hammond

et al. 1996; Graham et al. 2017). Increase in strahl width with radial distance was also successfully reproduced by an empirical model that assumed a pitch-angle scattering rate that was constant with time, distance, and electron kinetic energy (Owens et al. 2008). However, all three of the studies above produced different energy relations for strahl broadening per unit radial distance. Hammond et al. (1996) observed that strahl broadening per au steeply decreased with increasing strahl energy, Graham et al. (2017) observed that strahl broadening per au slightly increased with increasing strahl energy, and the Owens et al. (2008) model found that strahl broadening per au slightly decreased with increasing strahl energy. The energy relation found in this investigation does not agree with those of Hammond et al. (1996) or Owens et al. (2008), and although, like the Graham et al. (2017) study, we observe an increase in strahl broadening per au with electron energy, the increase observed is much steeper.

When comparing the results of these four studies, it is important to consider the possibility that slow and fast solar wind may produce differences in the strahl pitch-angle distribution, due to either in-transit processing or their solar origins. Some previous investigations have found that strahl beams are generally broader in the slow solar wind than the fast (e.g., Fitzenreiter et al. 1998), and it has also been shown that strahl width is greater when in proximity to IMF sector boundaries (Pilipp et al. 1987b). However, proximity to IMF sector boundaries is observed to result in strahl pitch-angle broadening that is independent of electron energy (Pilipp et al. 1987b) and therefore cannot explain the energy relation found in this investigation. Both the Hammond et al. (1996) observations and the Owens et al. (2008) model were made in fast solar wind streams. However, the Hammond et al. (1996) observations were made over a range of heliosphere latitudes, whereas the Owens et al. (2008) model assumed a constant heliolatitude. The Graham et al. (2017) observations were for unknown, but likely, mixed solar wind speeds obtained from 1999 to 2004. The results from this study were obtained from 1999 to 2002 and had average solar wind speeds ranging from ∼300 to 600 km s^{-1}. Both the observations made in this study and those of Graham et al. (2017) were for approximately constant heliolatitude, in the equatorial plane. Thus, it is likely that the average solar wind conditions seen by Graham et al. (2017) and this investigation were more similar to each other than those of Hammond et al. (1996) and Owens et al. (2008).

The energy relation produced by the Owens et al. (2008) model is solely a result of the suprathermal electrons having different velocities. The modeled scattering rate used in Owens et al. (2008) was constant with time, distance, and electron kinetic energy. Hence, the faster strahl electrons travel further along the modeled field in a given time and experience the same quantity of scattering but a greater adiabatic focusing effect. The observational results obtained in this investigation, Hammond et al. (1996), and Graham et al. (2017), which differ from the model and each other, cannot be explained solely by strahl time-of-flight effects. This suggests that the scattering mechanism or mechanisms for solar wind strahl may have an inherent energy dependence. Finally, we should note that Parker field line length estimates were not thought to be sufficient for the purpose of this current investigation, whereas the Owens et al. (2008) empirical model assumed Parker geometry. Thus, further work in which the model was altered to allow for heliospheric field lines that are longer or shorter than the predicted Parker values is needed to match strahl observations.

Although our results agree with the Graham et al. (2017) study, it is important to note the differences between the methods used in each case. This is particularly important because the results herein display a stronger strahl width broadening per au than reported in Graham et al. (2017). In this current study, we find strahl width broadening per au as a function of distance along the IMF path length by estimating the path length traveled by the strahl along the IMF from the Sun to 1 au. In contrast, Graham et al. (2017) found the strahl width broadening per au as a function of radial distance by fitting to the observed radial trends of strahl beam width from ∼1 to 5.5 au. In a Parker spiral field, the distance along the IMF path increases with radial distance from the Sun. For example, for solar wind with a speed of 500 km s^{-1}, the IMF path length would be 2.8 and 5.2 au at radial distances of 2 and 3 au from the Sun, respectively. Hence, if the Graham et al. (2017) results were measured in terms of IMF path length as opposed to radial distance, it is likely that the broadening per au would be an even lower value than when given in terms of radial distance. Thus, the difference in methods used does not explain the difference in results.

The observed strahl width broadening per au in the Graham et al. (2017) investigations was also thought to be relatively constant with heliospheric radial distance. Hence, if results were measured in terms of IMF path length as opposed to radial distance, this conversion would also result in a broadening per au along the IMF path length that decreased with radial distance from the Sun. It is expected that the effect of adiabatic focusing on the strahl beam will decrease with radial distance, due to the longer path length traveled along the IMF by the electrons for a given change in radial distance and hence in IMF strength. Therefore, the approximately constant radial broadening of strahl beam width with radial distance may be due to the strahl scattering mechanism decreasing with radial distance in conjunction with the effect of adiabatic focusing. Hence, comparison of the energy relation for strahl broadening per au found in this study and Graham et al. (2017) suggests that the dominant scattering mechanism, resulting in the observed energy relation, may have a stronger effect within 1 au than it does beyond it.

There are a number of possible wave–particle interactions that may result in strahl scattering, and there are a number of different possible drivers for these fluctuations. In particular, resonant interactions with whistler-mode waves are frequently invoked as a likely scattering mechanism to explain strahl pitch-angle width broadening (e.g., Hammond et al. 1996; Fitzenreiter et al. 1998; Vocks et al. 2005; de Koning et al. 2006; Pagel et al. 2007; Anderson et al. 2012). Depending on the driver of the whistler-mode fluctuations, a different energy relation for strahl scattering can be expected (Saito & Gary 2007, and references therein). For example, a broadband whistler spectrum resulting from turbulent cascade could produce strahl beam width that increases with strahl energy (Saito & Gary 2007). Alternatively, a core electron temperature anisotropy (where $T_\perp/T_\parallel > 1$) could lead to the excitation of the whistler anisotropy instability, producing enhanced whistler fluctuations that result in strahl beam width that decreases with strahl energy. Hence, specific properties of the whistler-mode waves may, in part, explain the ostensibly conflicting energy

dependence observations. These suppositions are supported by observations of the presence of whistler-like fluctuations in the solar wind (e.g., Lacombe et al. 2014). However, another recent study found that the majority of whistler-mode waves propagate in the anti-sunward direction as opposed to the sunward direction required for resonant interaction with anti-sunward-propagating strahl (Stansby et al. 2016).

There have also been numerous investigations in which the strahl itself has driven instabilities that can result in scattering of the strahl beam via a number of different wave–particle interactions. For instance, whistler-mode waves generated by the electron heat flux instability could be a potential source for scattering (Gary et al. 1994). Another possibility is fluctuations resulting from the electron firehose instability (where $T_{\perp}/T_{\parallel} < 1$), for example, the Hellinger et al. (2014) study, which found that nonpropagating waves produced by this instability resulted in scattering of the strahl. These standing waves where then transformed into propagating whistler-mode waves that were then rapidly damped, resulting in perpendicular electron heating. It has also been shown that strahl-generated Lagmuir waves can produce scattering effects significant enough to broaden the solar wind strahl population (Pavan et al. 2013). Finally, anisotropy of the strahl electron velocity distribution can also result in a core-strahl system that is unstable to lower hybrid waves and results in pitch-angle diffusion of the strahl (Shevchenko & Galinsky 2010).

Another frequently evoked candidate for strahl scattering are obliquely propagating kinetic Alfvén waves (KAWs), which may be able to interact with the field-aligned strahl via Landau damping. These suggestions are strongly supported by observations of KAW-like fluctuations at small scales (e.g., Kiyani et al. 2012; Salem et al. 2012; Chen et al. 2013). It should also be noted that intense strahl scattering events have been observed at 1 au during intervals of oblique KAWs (Gurgiolo et al. 2012). However, we should also note that evidence for resonant scattering of strahl electrons during whistler-mode intervals have been observed (Kajdič et al. 2016). In a recent investigation into magnetic field turbulence in the solar wind between 1 and 200 Hz, it was found that during intervals that did not contain quasi-parallel whistler-mode waves, there was a strong correlation between the observed compressibility and the expected compressibility for KAWs (Lacombe et al. 2017).

Resonant interaction with broadband whistler fluctuations is thought to result in higher-energy strahl experiencing greater pitch-angle broadening (e.g., Vocks et al. 2005; Pagel et al. 2007; Saito & Gary 2007). Hence, this scattering mechanism may explain the greater broadening per au for higher-energy strahl observed in this paper and Graham et al. (2017). The effectiveness of whistler-mode scattering depends on the available wave power below the electron gyrofrequency (Vocks et al. 2005), and the wave power and the electron gyrofrequency decrease with radial distance (Hu et al. 1999). Hence, a decrease in scattering effects with radial distance may also be consistent with whistler-mode wave interaction as the primary strahl pitch-angle scattering mechanism. It has been shown that whistler-like fluctuations are present in the solar wind up to 10% of the time (e.g., Lacombe et al. 2014). However, we should also note that whistler-mode waves are certainly not the only possible scattering mechanism for strahl, and thus further investigation into the effectiveness and occurrence of wave–electron interactions in the solar wind is required.

Finally, in this study we examined the PVI during the strahl width observations, as it is possible for magnetic field variations to result in local scattering or blurring of the strahl beam. We found that there was no clear relation between average strahl width and the median or maximum PVI values from each event. Our results suggest that the observed increase in strahl width with IMF path length is related to in-transit effects in the solar wind between the Sun and 1 au, and that the average strahl widths observed for our events are not strongly related to local magnetic variation effects at the time of observation. However, we are not able to rule out the possibility that local fluctuations on the kinetic scale may effect the strahl widths observed, such as the intense, bursty strahl electron scattering forming a proto-halo population as observed by Gurgiolo et al. (2012).

5. Summary

In this study we use a novel method to investigate strahl evolution within 1 au using IMF path lengths estimated using electron and ion SEP trajectories. We find that average strahl width broadened with distance traveled along the IMF. We also find that strahl pitch-angle width broadening per au along the IMF path length increased with strahl energy. These observations imply that the average width of the strahl beam is related to the distance traveled along the IMF path length by the strahl and that the dominant strahl pitch-angle scattering mechanism likely has an inherent energy relation. Previous observations of strahl width with heliospheric radial distance from ∼1 to 5.5 au display a similar energy relation (Graham et al. 2017). However, the increase in the broadening per au with strahl energy is not as steep as found in this study, suggesting that the scattering rate may be higher closer to the Sun. Broadband whistler fluctuations resulting from a turbulent cascade could produce the required relation with energy and radial distance needed to explain these observations.

Observations within 1 au are key to fully understanding solar wind strahl and SEPs. In particular, particle observations at different radial distances within 1 au allow for the study of their evolution, and inference of their origins, before they have been subject to significant in-transit processing. Our energy relation result for strahl pitch-angle broadening presents a testable hypothesis for the upcoming *Parker Solar Probe* and *Solar Orbiter* missions. In 2018 and 2019, respectively, the *Parker Solar Probe* and *Solar Orbiter* spacecraft will be launched, providing a whole new set of SEP and strahl observations within 1 au (the *Parker Solar Probe* within 9 solar radii). *Solar Orbiter* in particular, with its comprehensive suits of remote-sensing and in situ instruments, has the potential to dramatically improve our understanding of the source regions of both energetic particles and the solar wind. The data returned by *Parker Solar Probe* and *Solar Orbiter* not only will allow for significant expansion of this study but also will greatly improve our understanding of the transport of solar energetic particles, evolution of solar wind strahl, and their scattering mechanisms.

G.A.G. is supported by a UCL IMPACT studentship. I.J.R. and C.J.O. are supported by the STFC Consolidated grant to MSSL, ST/N000722/1. We thank the *Wind* instrument teams for the provision of the data used in this study, in particular the

3DP EESA, 3DP SST, EPACT LEMT, and MAG team members. Data used in this study can be found at the NASA Coordinated Data Analysis Web (NASA CDAWeb, https://cdaweb.sci.gsfc.nasa.gov/index.html/). Finally, we gratefully acknowledge S. Bale, R. Lin, D. Reames, A. Szabo, T. Von Rosenvinge, and L. Wilson for the data sets provided on NASA CDAWeb.

ORCID iDs

G. A. Graham https://orcid.org/0000-0002-3769-2587
I. J. Rae https://orcid.org/0000-0002-2637-4786
C. J. Owen https://orcid.org/0000-0002-5982-4667
A. P. Walsh https://orcid.org/0000-0002-1682-1212

References

Anderson, B. R., Skoug, R. M., Steinberg, J. T., & McComas, D. J. 2012, JGRA, 117, a04107
Borovsky, J. E. 2010, JGRA, 115, a09101
Che, H., & Goldstein, M. L. 2014, ApJL, 795, L38
Chen, C., Boldyrev, S., Xia, Q., & Perez, J. 2013, PhRvL, 110, 225002
de Koning, C. A., Gosling, J. T., Skoug, R. M., & Steinberg, J. T. 2006, JGRA, 111, a04101
Feldman, W. C., Asbridge, J. R., Bame, S. J., Gosling, J. T., & Lemons, D. S. 1978, JGRA, 83, 5285
Feldman, W. C., Asbridge, J. R., Bame, S. J., Montgomery, M. D., & Gary, S. P. 1975, JGR, 80, 4181
Fitzenreiter, R., Ogilvie, K., Chornay, D., & Keller, J. 1998, GeoRL, 25, 249
Forsyth, R., Balogh, A., Horbury, T., et al. 1996, A&A, 316, 287
Gary, S. P., Scime, E. E., Phillips, J. L., & Feldman, W. C. 1994, JGRA, 99, 23391
Gosling, J., McComas, D., Phillips, J., et al. 1994, GeoRL, 21, 2271
Gosling, J. T., Baker, D. N., Bame, S. J., et al. 1987, JGRA, 92, 8519
Graham, G. A., Rae, I. J., Owen, C. J., et al. 2017, JGRA, 122, 3858
Gurgiolo, C., & Goldstein, M. L. 2017, AnGeo, 35, 71
Gurgiolo, C., Goldstein, M. L., Viñas, A. F., & Fazakerley, A. N. 2012, AnGeo, 30, 163
Haggerty, D. K., & Roelof, E. C. 2002, ApJ, 579, 841
Hammond, C., Feldman, W., McComas, D., Phillips, J., & Forsyth, R. 1996, A&A, 316, 350
Hellinger, P., Trávníček, P. M., Decyk, V. K., & Schriver, D. 2014, JGRA, 119, 59
Horaites, K., Boldyrev, S., Wilson, L. B., III, Viñas, A. F., & Merka, J. 2017, arXiv:1706.03464
Hu, Y. Q., Habbal, S. R., & Li, X. 1999, JGRA, 104, 24819
Hundhausen, A., Bame, S., Asbridge, J., & Sydoriak, S. 1970, JGR, 75, 4643
Isobe, T., Feigelson, E. D., Akritas, M. G., & Babu, G. J. 1990, ApJ, 364, 104
Kajdič, P., Alexandrova, O., Maksimovic, M., Lacombe, C., & Fazakerley, A. 2016, ApJ, 833, 172
King, J., & Papitashvili, N. 2005, JGRA, 110, A02104
Kiyani, K. H., Chapman, S. C., Sahraoui, F., et al. 2012, ApJ, 763, 10
Klassen, A. 2017, in Proc. 7th Solar Orbiter Workshop: Exploring the Solar Environs (unpublished), C#10-1
Krucker, S., Larson, D. E., Lin, R. P., & Thompson, B. J. 1999, ApJ, 519, 864
Lacombe, C., Alexandrova, O., Matteini, L., et al. 2014, ApJ, 796, 5
Lacombe, C., Alexandrova, O., & Matteini, L. 2017, ApJ, 848, 45
Landi, S., Matteini, L., & Pantellini, F. 2012, ApJ, 760, 143
Lepping, R., Acũna, M., Burlaga, L., et al. 1995, SSRv, 71, 207
Lie-Svendsen, Ø., Hansteen, V. H., & Leer, E. 1997, JGRA, 102, 4701
Lin, R., Anderson, K., Ashford, S., et al. 1995, SSRv, 71, 125
Maksimovic, M., Zouganelis, I., Chaufray, J.-Y., et al. 2005, JGRA, 110, a09104
Mazur, J., Mason, G., Dwyer, J., et al. 2000, ApJL, 532, L79
Nitta, N. V., Reames, D. V., DeRosa, M. L., et al. 2006, ApJ, 650, 438
Osman, K., Matthaeus, W., Gosling, J., et al. 2014, PhRvL, 112, 215002
Owens, M. J., Crooker, N. U., & Lockwood, M. 2013, JGRA, 118, 1868
Owens, M. J., Crooker, N. U., & Schwadron, N. A. 2008, JGRA, 113, a11104
Pagel, C., Gary, S. P., de Koning, C. A., Skoug, R. M., & Steinberg, J. T. 2007, JGRA, 112, a04103
Pavan, J., Viñas, A., Yoon, P. H., Ziebell, L. F., & Gaelzer, R. 2013, ApJL, 769, L30
Pilipp, W. G., Miggenrieder, H., Montgomery, M. D., et al. 1987a, JGRA, 92, 1075
Pilipp, W. G., Miggenrieder, H., Mühlhäuser, K. H., et al. 1987b, JGRA, 92, 1103
Reames, D. V. 1999, SSRv, 90, 413
Reames, D. V. 2013, SSRv, 175, 53
Saito, S., & Gary, S. P. 2007, GeoRL, 34, l01102
Salem, C., Howes, G., Sundkvist, D., et al. 2012, ApJL, 745, L9
Seough, J., Nariyuki, Y., Yoon, P. H., & Saito, S. 2015, ApJL, 811, L7
Shevchenko, V., & Galinsky, V. 2010, NPGeo, 17, 593
Smith, H. M., Marsch, E., & Helander, P. 2012, ApJ, 753, 31
Stansby, D., Horbury, T., Chen, C., & Matteini, L. 2016, ApJL, 829, L16
Stverak, S., Maksimovic, M., Travnicek, P. M., et al. 2009, JGRA, 114, a05104
Tan, L. C., Malandraki, O. E., Reames, D. V., et al. 2013, ApJ, 768, 68
Tan, L. C., Reames, D. V., Ng, C. K., Shao, X., & Wang, L. 2011, ApJ, 728, 133
Vocks, C., Salem, C., Lin, R. P., & Mann, G. 2005, ApJ, 627, 540
Von Rosenvinge, T., Barbier, L., Karsch, J., et al. 1995, SSRv, 71, 155
Wiedenbeck, M. 2011, Proc. ICRC 32 (Beijing), 10, 208